Magnetic Properties of Bulk Nanocrystalline Cobalt Ferrite Obtained by High-Pressure Field Assisted Sintering

Angelica Baldini[1], Michele Petrecca[2,3], Claudio Sangregorio[3], Umberto Anselmi-Tamburini[1]

[1]Dipartimento di Chimica, Università di Pavia, V.le Taramelli 12, 27100 Pavia, Italy
[2]Dipartimento di Chimica, "Ugo Schiff", Università degli Studi di Firenze, via della Lastruccia 3-13, I-50019 Sesto Fiorentino, and Consorzio INSTM, via Giusti 9, I-50121 Firenze, Italy
[3]I.C.C.O.M. - CNR, via Madonna del Piano 10, I-50019 Sesto Fiorentino, and Consorzio INSTM, via Giusti 9, I-50121 Firenze, Italy

E-mail: angelica.baldini01@universitadipavia.it

Received xxxxxx
Accepted for publication xxxxxx
Published xxxxxx

Abstract

We present here an investigation aimed at exploring the role of the microstructure on the magnetic properties of nanostructured cobalt ferrite. Bulk, almost fully dense, nanograined ferrites have been obtained starting from nanopowders prepared by a simple, inexpensive, water-based, modified Pechini method. This synthesis yielded largely aggregated, pure single-phase cobalt ferrite nanoparticles of ca. 35 nm average size, which have been then densified by high-pressure field-assisted sintering (HP-FAST). Different sintering conditions (pressure up to 650 MPa and temperature up to 800 °C) and procedures have been used on both as-prepared and milled nanopowders in order to obtain materials with a spectrum of complex microstructures. In all cases, the sintering process did not produce any change in the phase composition. At the same time, using a high uniaxial pressure in combination with relatively low sintering temperatures and times, allowed for obtaining a high degree of densification while preserving the nanometric size of the crystallites. Moreover, we observed that in the densified materials the best magnetic properties are not necessarily associated with a more uniform microstructure, but rather arise from a delicate balance between moderate aggregation, grain size and high density.

Keywords: Nanopowders, sintering, bulk material, cobalt ferrite, microstructure

1. Introduction

Hard magnetic materials represent a crucial component in a large number of relevant technological applications. The best hard magnetic properties are generally presented by metallic alloys, such as rare earth-based alloys [1-3] or, to a minor extent, ALNICO. However, the limited availability and the rising cost of rare earth metals [4, 5], together with their low corrosion resistance and high environmental impact, have recently fuelled the interest towards alternative magnetic materials. Ceramic oxides represent an interesting alternative, as they do not suffer from oxidation or corrosion, are widely available, inexpensive, and environmentally friendly. However, the magnetic properties of oxides are still largely inferior to the one shown by rare earth-based magnetic alloys. On the other hand, it has been shown that the nanostructure can significantly alter the magnetic properties of these oxides. [6-9] The nanostructure can drastically modify the magnetization, the magnetic anisotropy, and the ordering (Curie and Néel) temperature of these materials. [10,11]
In particular, it has been recognized that the highest coercivity is obtained at the boundary between single and multidomain materials, which for the most common magnetic materials falls in the 10-150 nm range. Such property is appealing for

realizing permanent magnets since a large coercivity is required to sustain the residual magnetization.

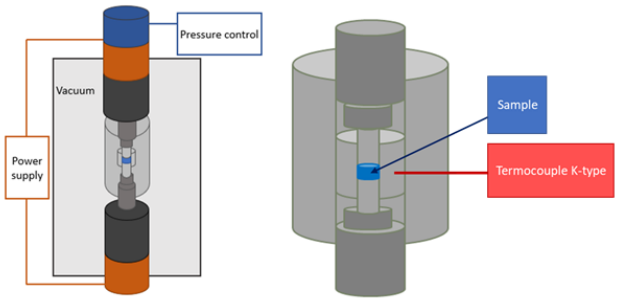

Figure 1. (Left) schematic of the HP-FAST apparatus used in this investigation. (Right) schematic of the dual-stage high-pressure die used for the densification of the nanopowder.

The unusual magnetic properties exhibited by ferrite nanoparticles (NP) have spurred a broad scientific interest over the last decades. [12-15] Ferrites are compounds with a spinel crystal structure and general formula AFe_2O_4, with A being a divalent cation. [16,17] If compared to their micrometric counterpart, nano sized ferrites possess unusual saturation magnetization and higher coercive field. [18-20] One of the most promising ferrites is represented by the cobalt magnetite. Recently, 40 nm $Co_{0.6}Fe_{2.4}O_4$ nanoparticles have been proposed for the realization of permanent magnets (PM). [18] Values of M_s above 80 Am^2kg^{-1} and of H_c around 238 kAm^{-1} have been reported at room temperature for nanoparticles of this material. [18]
The magnetic properties of monodispersed nanopowders or nanocrystals of ferrites have been extensively investigated [21-28]. However, most technological applications require the magnetic materials to be in bulk form. For this reason, the production of bulk samples retaining the magnetic properties of the nanopowders is highly desirable. Despite that, the number of reports on bulk cobalt ferrite deriving from the sintering of nanopowders are still quite limited. [29-33] The main challenge in realizing these materials is represented by the control of the grain growth during the sintering process. It has been recently shown that innovative fast sintering methods, such as Field Assisted Sintering (FAST) or Spark Plasma Sintering (SPS), offer the possibility to obtain the densification of nanopowders with a minimal grain growth, particularly when the process is performed under high uniaxial pressures (up to 1 GPa). [34-36] This approach, coupling high pressures with fast heating cycles, has been demonstrated to be particularly effective even when low-quality nanopowders, presenting a high level of aggregation, are used. [37] This last point is particularly relevant for the production of materials in bulk form. In most cases, in fact, the studies on the magnetic properties of ferrite nanomaterials have been performed on high-quality, monodisperse nanopowders. [21,38,39] The synthesis of these nanopowders, however, is generally expensive, time-consuming, and offer low yields. As such, other approaches must be pursued for the production of the large quantities of nanopowders required for the production of bulk materials. On the other hand, simpler, water-based, high-yield approaches, such as the Pechini method, [40] generally produce badly aggregated nanopowders that are not ideal for sintering.

This work aims to explore the possibility of preparing bulk nanostructured $CoFe_2O_4$ samples applying high-pressure field-assisted sintering (HP-FAST) to the densification of nanopowders produced using a simple, low-cost approach, based on a modified Pechini method. It also aims to investigate the role of the microstructure of sintered materials on their magnetic properties.

2. Methods

2.1 Synthesis of Co-ferrite NP

Cobalt ferrite nanopowder has been synthesized using a modified Pechini method [40]. $Fe(NO_3)_3 \cdot 9H_2O$, $Co(NO_3) \cdot 6H_2O$ with cationic stoichiometry 2:1 and citric acid, with a 1:1 molar ratio to the cations, were dissolved in 60 mL of distilled water. The solution was kept under stirring at 80 °C for 16 h until a brown gel was formed. This gel was dried in a furnace at 120 °C for 2 h, then calcined at 600 °C for 1 h in an alumina boat. The reaction product was represented by a strongly aggregated black powder. In some cases, a mild milling treatment was performed using a FRITSCH Premium line P7 planetary ball-miller with WC jars and balls. The jars were cleaned previously by milling 7 mL of SiO_2 powder at 400 rpm for 30 min.

2.2 Sintering process

Bulk nanostructured samples were obtained using the home-made high-pressure field-assisted sintering (HP-FAST) apparatus, shown in Figure 1. The apparatus allows a maximum uniaxial load of 10 tons, driven by a pneumatic system controlled by a PID logic. An AC power supplier allows obtaining up to 5000 A of current with a maximum applied voltage of 6 V. Dual-stage dies allowing to achieve uniaxial pressures up to 1 GPa have been used in this study. In these dies, most of the current flow through an external element, where most of the heat is generated, made of high-density graphite. A second internal die, made out of SiC or WC, allow achieving the high pressure. The combination of high pressures and high heating rates (200 °C/min) allows achieving high densification levels with minimum grain growth. In a typical experiment, 0.150 g of nanopowders were placed in the dual-stage die with an internal diameter of 5 mm. The die was inserted in the HP-FAST apparatus and connected to a K-type thermocouple placed in its lateral wall. The HP-

FAST chamber was evacuated to a pressure of 10 Pa. Two different experimental procedures have been followed. In one case, a moderate uniaxial pressure (200 MPa) was initially applied to the sample, and the temperature was increased at a rate of 200 °C/min up to the designated sintering temperature (T_{sint}, investigated range: 500 – 800 °C). The pressure was then rapidly increased to the nominal value (P_{sint}, investigated range: 400 - 600 MPa). The sample was maintained under these conditions for 5 min.

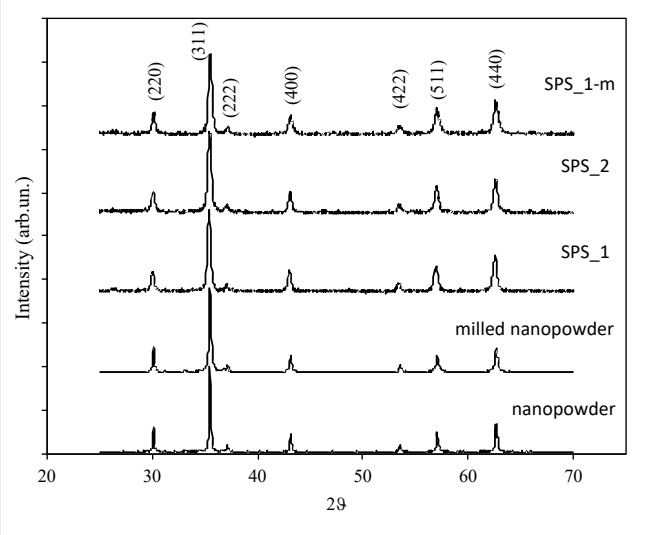

Figure 2. XRD patterns of the cobalt ferrite nanopowders and of samples sintered at 575°C under a pressure of 650 MPa using the three different procedures described in the text.

At the end of the sintering cycle, the pressure was quickly released, and the power supply turned off. In the following, the samples obtained using this procedure are labeled as SPS_1. In the second procedure, the sintering pressure was applied directly at the beginning of the process and maintained constant throughout the sintering cycle. The same range of pressure and sintering temperature as in the SPS_1 series were investigated. The label SPS_2 indicates these samples. The label SPS_1-m indicates samples obtained through the procedure SPS_1 when milled powders were used. In all cases, the sintered samples were discs of 5 mm in diameter and 1 mm thick.

2.3 Samples characterization

The densities of the sintered samples were determined at room temperature using the Archimedes method by immersion in EtOH. The theoretical density of the cobalt ferrite was evaluated from the crystallographic data. [41] The structural characterization was made by X-ray diffraction. XRD data were acquired on a Bruker D8 Advance diffractometer with Bragg-Brentano geometry, using a step size of *0.03°* (*2θ*) and an acquisition time of *5s* per step. The samples' microstructural characterization was performed using a high-resolution scanning electron microscope (SEM, TESCAN Mira 3) operated at 15-25 kV. The content of Fe and Co was determined by energy dispersive spectrometry (EDX, EDAX). In some cases, the microstructural characterizations of the sintered materials have been performed on ceramographic sections. In this case, the samples were embedded in epoxy resin (Buehler EpoThin 2 Resin), sectioned, and polished. Before SEM analysis, all samples were coated with a carbon film using a Cressington carbon coater HR 208. The grain size of both nanopowder and sintered samples were determined by XRD, using the Scherrer equation. Sintered samples have been grounded before the analysis. SEM evaluation of the grain size was performed using the software ImageJ. The reported values represent the average of at least 200 grains for each sample.

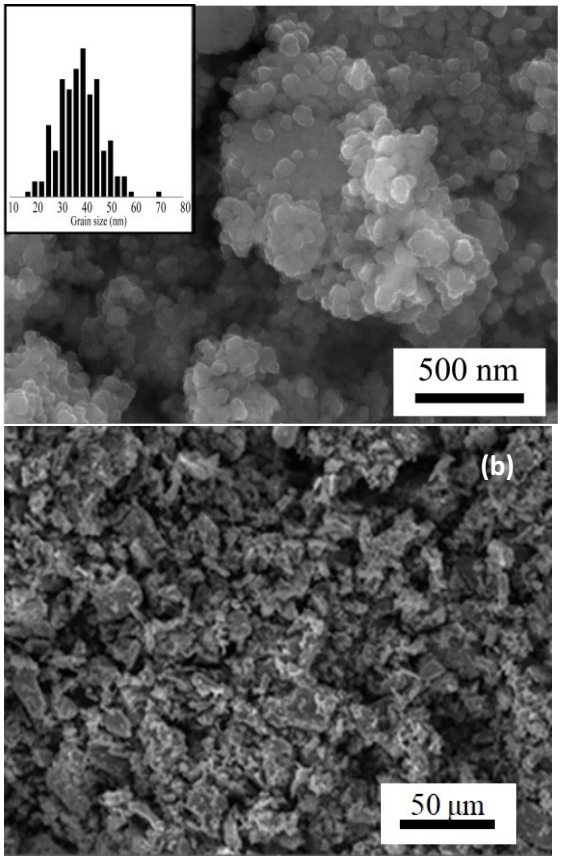

Figure 3. (a) high-magnification and (b) low-magnification SEM images of the cobalt ferrite nanopowder.

In the case of sintered materials, the measure has been performed on fracture surfaces. The magnetic measurements were carried out at room temperature on sintered discs, inserted with the axial direction (i.e., the normal to the plane of the disc) perpendicular to the applied DC field. The magnetic response was recorded as a function of the applied field using a Physical Property Measurement System (PPMS)

with a Vibrating Sample Magnetometer (VSM) by Quantum Design Inc. The energy product (BH_{max}) value was estimated from the BH curve, using the disc measured density and a demagnetizing factor of 0.1, according to the value reported in the literature for the same geometry and orientation. [42]

3. Results and Discussion

3.1 $CoFe_2O_4$ nanopowders

The nanopowder synthesized using the modified Pechini method were single-phase $CoFe_2O_4$, as evidenced by the XRD pattern reported in Figure 2. The lattice parameter *a*, calculated using the Pawley method, [43] was 0.8382(2) nm,

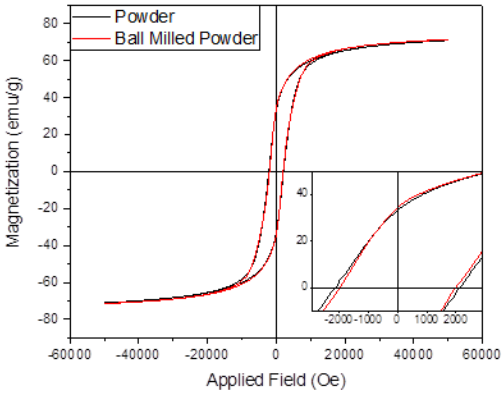

Figure 4. Hysteresis loops of the as-synthesized (black curve) and ball-milled nanopowders (red curve).

a value comparable with that reported in the literature for stoichiometric cobalt ferrite. [41] The crystallite size, as calculated from the XRD pattern, was 35(2) nm. The value was confirmed by HR-SEM analysis (Figure 3a). This grain size is a low limit of the estimation (no instrumental broadening) and is very close to the value at which cobalt ferrite energy product has been reported to be maximum (40 nm) [18]. As shown in figure 3a, in our case the grains did not show any evidence of faceting. Low-magnification images of the nanopowder (Figure 3b) evidenced the presence of an extensive aggregation. The magnetic hysteresis loop of the nanopowder recorded at room temperature is shown in Figure 4, while the magnetic properties are summarized in Table 1. The values for saturation magnetization (M_S, 71 Am^2kg^{-1}), remnant magnetization (M_R, 33 Am^2kg^{-1}), and coercive field (H_C, 171.1 kAm^{-1}) are comparable with the one reported in the literature for cobalt ferrite nanopowders obtained by various synthesis methods. [44-46] The BH_{max}, calculated considering the density of the stoichiometric cobalt ferrite (5.22 g cm^{-3}), and the sample shape (hand-pressed pellet in Teflon tape oriented with the normal perpendicular to the applied field, demagnetizing factor=0.05), was 6.0 kJ/m^3.

The aggregation level decreased considerably after ball milling (see SI for SEM images), while the phase composition remained unchanged. The lattice parameter also remained constant (0.8384(2) nm), as the crystallite size. The hysteresis loop recorded at room temperature on the milled powders is also shown in Figure 4, while the magnetic properties are summarized in Table 1. The saturation magnetization and the remanence remained almost unchanged (72 Am^2kg^{-1} and 34 Am^2kg^{-1}, respectively), while it was observed a slight decrease of the coercivity, from 171.1 to 159.1 kAm^{-1}. The BH_{max} value was 6.2 kJ/m^3. These little differences are within the technique's error range (± 3 % on the magnetic moment value) and confirm that the milling process did not affect the nanomaterial crystallinity but decreased only its aggregation level.

3.2 $CoFe_2O_4$ sintered samples

Sintered samples were obtained using several combinations of temperature and pressure on both pristine and milled nanopowders. It must be noted that the values of uniaxial pressures used in this study are well above the typical values used in SPS or FAST practice. Such high-pressure values are essential for obtaining high relative densities using sintering temperature and sintering time low enough to avoid significant grain growth. Sintering times of only 5 minutes have been indeed used throughout this work.

The sintering process did not produce any change in the phase composition of the material, that remained in all cases single-phase cobalt ferrite, as shown in Figure 2. The lattice parameters remained unchanged (0.8385(2) nm). The dependence of the sample relative density on the sintering temperature is reported in Figure 5 for an applied pressure of 500 MPa, as a representative case.

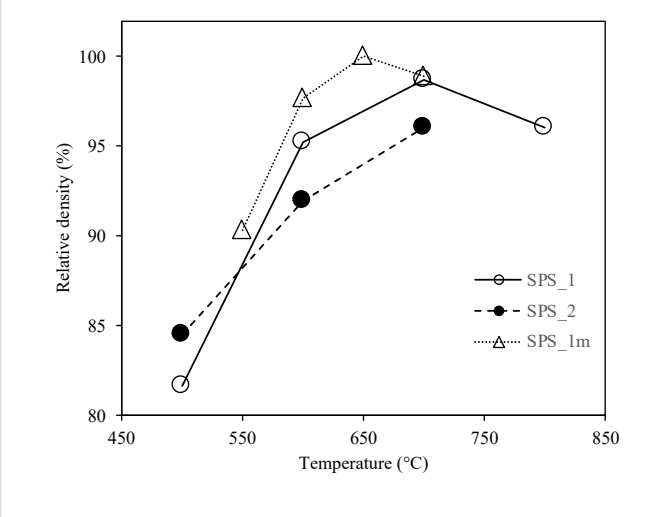

Figure 5. Relative density for samples obtained using the sintering procedures SPS_1, SPS_2, and SPS_1-m at different temperatures under an uniaxial pressure of 500 MPa.

Table 1. Structural and magnetic properties for the nanopowders and of samples densified at T = 575°C and P = 650 MPa using the three different procedures described in the text. Errors on experimental measurement of M_S and H_C is estimated less than 1%.

	H_c (kAm^{-1}) 300K	M_s (Am^2kg^{-1}) 300K	M_r (Am^2kg^{-1}) 300K	BH_{max} (kJ/m^3) 300K	Grain size SEM (nm)	CrystalSize XRD (nm)	Relative density (%)
Powder	171.1	71	33	6.0	35(5)	35(2)	-
Milled Powder	159.1	72	34	6.2	35(5)	35(2)	-
SPS_1	82.8	77	37	5.5	42(6)	35(5)	94
SPS_2	79.6	73	30	3.8	39(5)	25(5)	93
SPS_1-m	165.0	77	41	8.2	49(10)	35(5)	96

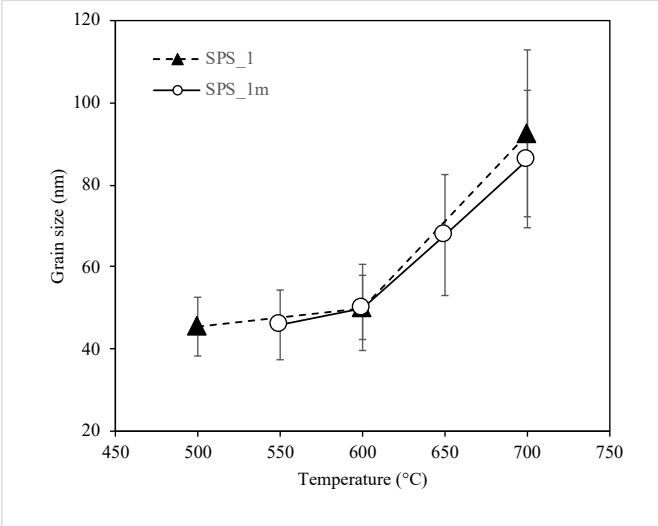

Figure 6. SEM grain size of samples sintered using the procedures SPS_1 and SPS_1-m at different temperatures under a uniaxial pressure of 500 MPa.

All samples obtained from the as prepared nanopowder and densified at T ≥ 600 °C presented a relative density above 93 %, reaching a maximum value of 98 % at 700 °C.

Milled nanopowders, presenting a reduced aggregation, densified at lower temperatures (Figure 5). In this case, almost full density was achieved at temperatures just above 600 °C using a pressure of 500 MPa.

Figure 6 shows as the apparent grain size, determined by HR-SEM, increases rapidly with temperature. The grain size, in fact, increased from 45(8) nm to 92(20) nm when the temperature was increased from 500 °C to 700 °C for samples obtained using the SPS_1 procedure. In samples obtained using the SPS_1-m procedure, the grain size increased from 46(8) to 86(16), raising the temperature from 550°C to 700 °C.

No change in the crystallite sizes obtained from XRD is observed in samples sintered at 575°C (Table 1).

This observation confirms that the very mild sintering conditions we used for densifying the samples reported in Table 1 do not produce any real growth of the individual nanograins, but only a strong bonding among them.

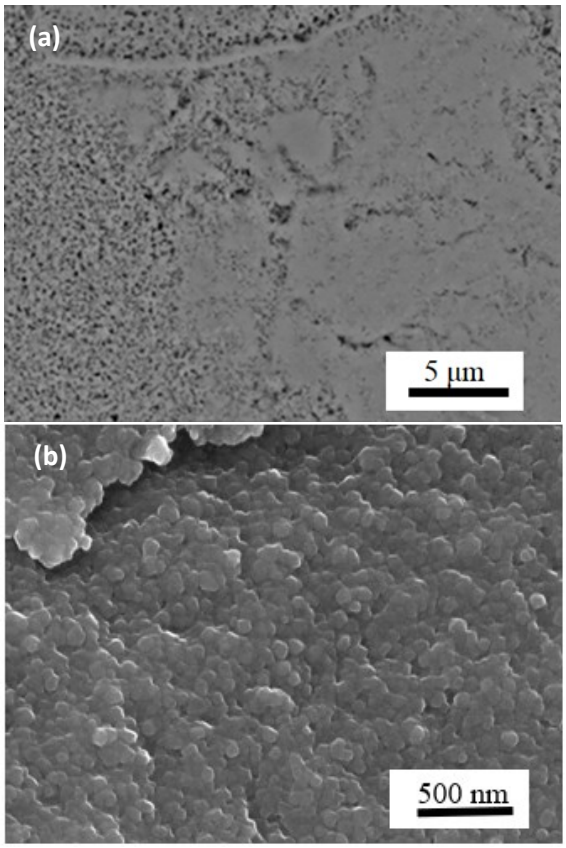

Figure 7. SEM images of a sample sintered using the procedure SPS_1 at 575°C under a pressure of 650 MPa. (a) polished section (BSE); (b) fracture surface.

For this reason, we choose T = 575 °C and P = 650 MPa as the optimal sintering conditions for our samples. Using these conditions, the relative densities lay between 96% and 93%, while the grain size was still very closed to the one shown by the starting nanopowder.
The microstructure of the sintered materials was strongly dependent on the type of nanopowders and on the sintering procedure.

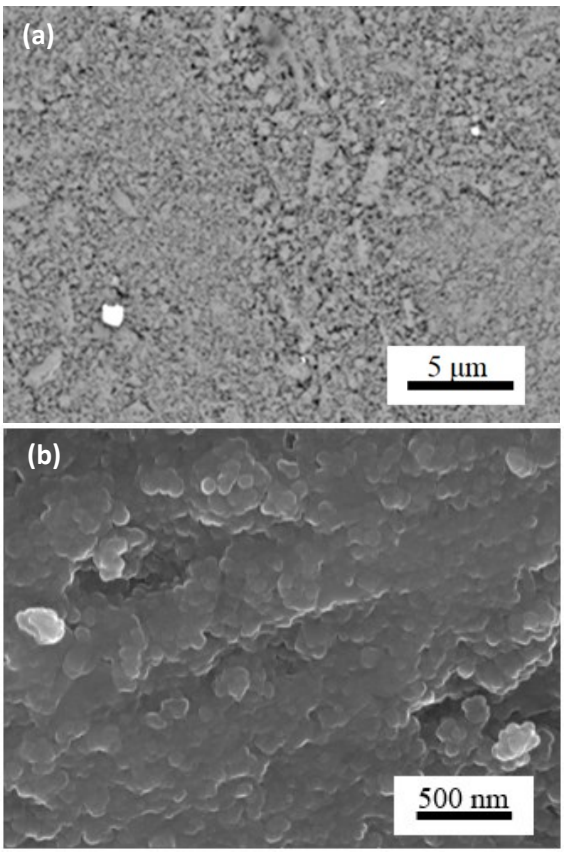

Figure 8. SEM images of a sample obtained from milled nanopowders and sintered using the procedure SPS_1-m at 575°C and 650 MPa. (a) polished section (BSE); (b) fracture surface. The bright spots are due to WC contamination deriving from the milling medium.

Bulk samples obtained from unmilled nanopowder, using the procedure SPS_1 presented a quite inhomogeneous microstructure. Figure 7 shows the SEM-BS image of the polished cross-sections of a sample sintered at 575 °C under a pressure of 650 MPa. The images show some fully dense areas, micrometric in size, surrounded by regions presenting residual nanoporosity. The fully dense areas present dimensions that are comparable to the size of the aggregates present in the starting nanopowder. No macro or mesoporosity was observed. The milling treatment of the nanopowders improved the microstructural homogeneity considerably. Figure 8 shows the microstructure of a sample obtained using the same sintering conditions (575°C and 650 MPa) and the procedure SPS_1-m. The large aggregates cannot be observed anymore. Only smaller aggregates, sub-micrometric in size, are present together with some residual nanoporosity. Notably, samples deriving from milled nanopowders show always some contamination by WC, deriving from the milling medium. The presence of this impurity was confirmed the EDX analysis.

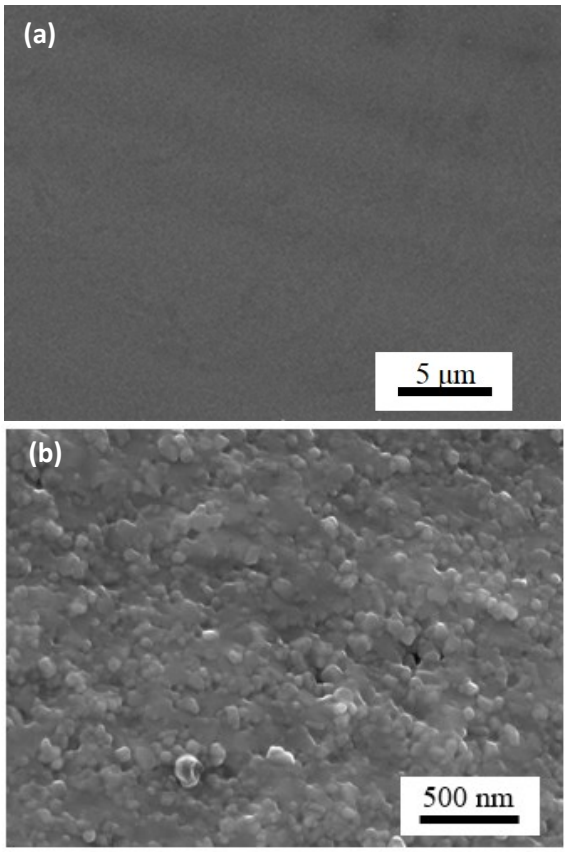

Figure 9. SEM images of a sample sintered using the procedure SPS_2 at 575°C and 650 MPa. (a) polished section (BSE); (b) fracture surface.

A much more uniform microstructure was obtained using the densification procedure SPS_2. In this case, the maximum uniaxial pressure was applied initially on unmilled nanopowders and it was maintained throughout the entire sintering cycle. Using this approach, the aggregates were drastically reduced, as they were probably effectively crushed in the early stages of the process, where plastic deformation was still not possible. [47] Figure 9 shows the cross section of one of these samples sintered at 575°C and 650 MPa of pressure. The microstructure looks remarkably uniform despite the extensive aggregation present in the starting nanopowders. In all these samples, however, the high-resolution SEM images shows a very similar grain size.

We characterized the magnetic properties of samples obtained using the same sintering conditions (T_{sint} = 575 °C and P_{sint} = 650 MPa), but presenting the quite different microstructures shown previously and deriving from the three sintering procedures SPS_1, SPS_2, and SPS_1-m.

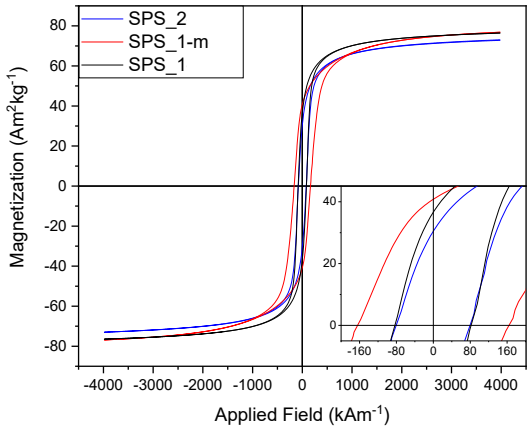

Figure 10. Hysteresis loop at room temperature for samples sintered at 575°C and 650 MPa using the procedures SPS_1, SPS_2, and SPS_1-m.

The magnetic properties of theses optimized samples are summarized in Table 1, while Figure 10 shows the corresponding hysteresis loops measured at room temperature. It is first interesting to compare the properties of the sintered samples with that of the loose nanopowders. For samples obtained using the procedure SPS_1-m and SPS_1, both M_S and M_R at 300 K increased after sintering, reaching the highest values of 77 Am^2kg and 41 Am^2kg, respectively. No increase with respect to the pristine nanopowders was instead observed for the sample obtained using the procedure SPS_2. On the other hand, the coercive field decreased in the sintered samples SPS_1 and SPS_2 down to 82.8 and 79.6 kAm^{-1}, respectively, but not in SPS_1-m, where it remained comparable to the starting nanopowders (165 kAm^{-1}). These results can be explained considering that the thermal treatment induces on one hand the increase of magnetic ordering, and on the other the decrease of the number of pinning center at the grain interfaces, making the demagnetization process more energetically favored (i.e. it decreases the coercivity and the reduced remanence, M_R/M_S). However, the milling process breaks down the number of large aggregates in the sintered samples, preserving the pinning centers and strongly reducing the relevance of the latter effect. Consequently, the maximum energy product, evaluated using the density of the sintered pellet, is considerably decreased in comparison with the starting nanopowdres in SPS_2 (3.8 kJ/m^3), slightly decreased in SPS_1 (5.5 kJ/m^3), but considerably increased (8.2 kJ/m^3) in the sample SPS_1m. However, it must be noted that the BH_{max} relative to the nanopowders is only an estimate obtained using the particle density and not the actual density of the pellet (unknown) and is surely overestimated. Finally, it is worth mentioning that the values of the magnetic parameters we observed in our sintered samples were, in most cases, superior to those reported in the literature for densified cobalt ferrite materials [29-33,45,46], as shown in Table 2. Particularly relevant is the considerably higher values of H_C observed in the case of the sintered sample obtained from milled nanopowder (SPS_1-m). This hard character arises from the size of the grain, that is not altered by the SPS compaction and remains close to the value where the reversal process in cobalt ferrite requires the largest energy,[18] and from the high density.

These results confirm that the microstructure plays a crucial role in determining the final sintered product magnetic properties. Surprisingly, a very uniform microstructure does not seem to be particularly advantageous. The sample SPS_2, which is characterized by a very homogeneous microstructure, presents the lowest value of BH_{max}, a value considerably inferior than the one shown by the sample SPS_1, which present a comparable relative density and grain size, but a very inhomogeneous microstructure. On the other hand, the sample SPS_1-m shows the best magnetic properties, in terms of coercive field and remanence, although the material presents a significant submicrometric aggregation and contains some contamination from the milling medium.

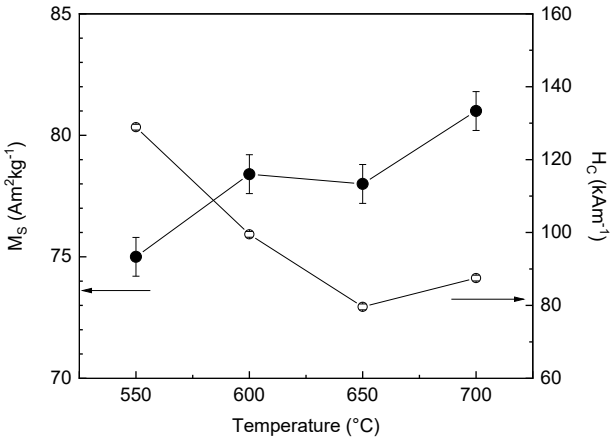

Figure 11. Coercive field (empty symbol, right scale) and saturation magnetization (full symbols, left scale) for samples sintered using the procedure SPS_1-m at different temperatures under a uniaxial pressure of 650 MPa. For H_C values error bars are smaller than symbol size.

This sample, indeed, presents the optimal compromise between moderate aggregation, high relative density (96%) and small grains size, compromise that maximizes the loop area of SPS_1-m and consequently the BH_{max}.

Some further insight into the microstructure role in defining the magnetic properties can be obtained from the data in Figure 11. In these figures, the coercive field and saturation magnetizations for the material presenting the best combination of magnetic properties (SPS_1-m) are reported as a function of the sintering temperature in the 550-700 °C range. It can be observed as the coercive field and the magnetization present an opposite trend. Increasing the sintering temperature, the coercive field reduced to a value that is almost half of that shown by the starting nanopowder, while M_S increased slightly.
This behavior is related to the increase of the grain size and of the order of the spin structure with the sintering temperature.

It is worth to stress that when sintering temperature are kept below 650 °C (with a relative density higher than 90 %), a H_C higher than the one reported so far in the literature was obtained, while the M_S values are comparable. This large coercivity can be ascribed to the preservation of the nanometric grains in the sintered product.

Table 2. Comparison between the magnetic properties of the materials produced in this study and the literature data.

	H_c (kAm^{-1}) 300K	M_s (Am^2kg^{-1}) 300K	Grain size (nm)	Relative density (%)
This study	59.7-171.1	70-86	45-150	88-100
[31]	19.0	78.9	120	97
[31]	53.0	70.0	100	97
[32]	50.9	79.3	28	91
[29]	17.7	83	71	97
[30]	46.1	51	10	92
[30]	41.8	69	12-15	93
[30]	52.5	70	40-50	93
[33]	65.7	82.1	<200	/

4. Conclusions

We demonstrated that high-pressure field-assisted sintering (HP-FAST) allows obtaining almost fully dense nano sized cobalt ferrite even when the starting nanopowders present a significant aggregation. The use of high uniaxial pressures, up to 600 MPa, allows removing all macro- and mesoporosity even using relatively low sintering temperatures and sintering times reduced to few minutes. The magnetic properties of starting nanopowders are almost entirely retained in the bulk samples when a mild milling treatment is used before compaction. We found that while the presence of large aggregates affects the magnetic properties of the sintered material, some level of microstructural heterogeneity helps to maintain the magnetic properties of the nanopowders. Our results confirm the complex role that the microstructure plays in defining the magnetic characteristics of bulk nanostructured sintered magnetic materials.

Acknowledgments

The author sincerely thank Dr. C. de Julián Fernandez for scientific discussion on magnetic data. We gratefully acknowledge the CISRiC at the University of Pavia to use theR-SEM facility and the European Commission for funds through project H2020 No. 720853 (Amphibian).

References

1. Elliott, R. Magnetic Properties of Rare Earth Metals. *Springer Science & Business Media*, (2013).
2. Koehler, W. C. Magnetic Properties of Rare-Earth Metals and Alloys. *J. Appl. Phys.* **36**, 1078–1087 (1965).
3. Sagawa, M., Fujimura, S., Yamamoto, H. & Hiraga, K. Permanent magnet materials based on the rare earth-iron-boron tetragonal compounds. *IEEE Trans. Magn.* **20,** 1584-1589 (1984)
4. Massari, S. & Ruberti, M. Rare earth elements as critical raw materials: Focus on international markets and future strategies. Resour. Policy 38, 36–43 (2013).

5. Gutfleisch, O., Willard, M.A., Brück, E., Chen, C.H., Sankar, S. G. & Liu J.P. Magnetic materials and devices for the 21st century: stronger, lighter, and more energy efficient. *Advanced Materials* **23**(7), 821-842 (2011):.
6. Gleiter, H. Nanostructured materials: basic concepts and microstructure. Acta Mater. 48, 1–29 (2000).
7. Moriarty, P. Nanostructured materials. Rep. Prog. Phys. 64, 297 (2001).
8. Cain, M. & Morrell, R. Nanostructured ceramics: a review of their potential. *Appl. Organomet. Chem.* **15**, 321–330 (2001)
9. Fernández-García, M., Martínez-Arias, A., Hanson, J. C. & Rodriguez, J. A. Nanostructured Oxides in Chemistry: Characterization and Properties. *Chem. Rev.* **104**, 4063–4104 (2004).
10. Trohidou, K. N. *Magnetic Nanoparticle Assemblies*. (CRC Press, 2014)
11. Issa, B., Obaidat, I., Albiss, B. & Haik, Y. Magnetic Nanoparticles: Surface Effects and Properties Related to Biomedicine Applications. *Int. J. Mol. Sci.* **14**, 21266–21305 (2013)
12. Mathew, D. S. & Juang, R.-S. An overview of the structure and magnetism of spinel ferrite nanoparticles and their synthesis in microemulsions. *Chem. Eng. J.* **129**, 51–65 (2007).
13. Pacakova, B., Kubickova, S., Reznickova, A., Niznansky, D. & Vejpravova, J. Spinel Ferrite Nanoparticles: Correlation of Structure and Magnetism. *Magn. Spinels - Synth. Prop. Appl.* (2017) doi:10.5772/66074.
14. Muthukumaran, T. & John Philip. A facile approach to synthesis of cobalt ferrite nanoparticles with a uniform ultrathin layer of silicon carbide for organic dye removal. *J. Mol. Liquids* **317**, 114110 (2020).
15. Anushree, C. & Philip J. Efficient removal of methylene blue dye using cellulose capped Fe_3O_4 nanofluids prepared using oxidation-precipitation method. *Colloids and Surfaces A: Physicochemical and Engineering Aspects*, **567**, 193-204 (2019).
16. Carta, D. Casula, M. F., Falqui, A., Loche, D., Mountjoy, G., Sangregorio, C. & Corrias, A. A Structural and Magnetic Investigation of the Inversion Degree in Ferrite Nanocrystals MFe_2O_4 (M = Mn, Co, Ni). *J. Phys. Chem. C* **113**, 8606–8615 (2009).
17. Verwey, E. J. W. & Heilmann, E. L. Physical Properties and Cation Arrangement of Oxides with Spinel Structures I. Cation Arrangement in Spinels. *J. Chem. Phys.* **15**, 174–180 (1947).
18. López-Ortega, A., Lottini, E., Fernández, C. de J. & Sangregorio, C. Exploring the Magnetic Properties of Cobalt-Ferrite Nanoparticles for the Development of a Rare-Earth-Free Permanent Magnet. *Chem Mater.* **27**, 4048–4056 (2015).
19. Vasilakaki, M., Ntallis, N., Yaacoub, N., Muscas, G., Peddis, D. & Trohidou, K.N. Optimising the magnetic performance of Co ferrite nanoparticles *via* organic ligand capping. *Nanoscale* **10**, 21244–21253 (2018).
20. Rondinone, A. J., Samia, A. C. S. & Zhang, Z. J. Superparamagnetic Relaxation and Magnetic Anisotropy Energy Distribution in $CoFe_2O_4$ Spinel Ferrite Nanocrystallites. *J. Phys. Chem. B* **103**, 6876–6880 (1999).
21. Baldi, G., Bonacchi, D., Innocenti, C., Lorenzi, G. & Sangregorio, C. Cobalt ferrite nanoparticles: The control of the particle size and surface state and their effects on magnetic properties. *J. Magn. Magn. Mater.* **311**, 10–16 (2007).
22. Joshi, H. M., Lin, Y. P., Aslam, M., Prasad, P. V., Schultz-Sikma, E. A., Edelman, R., Meade, T. & Dravid, V. P. Effects of Shape and Size of Cobalt Ferrite Nanostructures on Their MRI Contrast and Thermal Activation. *J. Phys. Chem. C* **113**, 17761–17767 (2009).
23. Li, S., John, V. T., O'Connor, C., Harris, V. & Carpenter, E. Cobalt-ferrite nanoparticles: Structure, cation distributions, and magnetic properties. *J. Appl. Phys.* **87**, 6223–6225 (2000).
24. Ayyappan, S., Panneerselvam, G., Antony, M. P. & Philip, J. High temperature stability of surfactant capped CoFe2O4 nanoparticles. *Mater. Chem. Phys.* **130**, 1300–1306 (2011).
25. Ayyappan, S., Paneerselvam, G., Antony, M. P. & Philip, J. Structural stability of $ZnFe_2O_4$ nanoparticles under different annealing conditions. *Mater. Chem. Phys.* **128**, 400–404 (2011).
26. Yoo, H.-I. Phase stability and ionic transference number of a ferrite spinel, $Mn_{0.54}Zn_{0.35}Fe_{2.11}O_4$. *Solid state ion*. **84**, 77-88 (1996).
27. Mazarío, E., Herrasti, P., Morales, M. P. & Menéndez, N. synthesis and characterization of $CoFe_2O_4$ ferrite nanoparticles obtained by an electrochemical method. *Nanotechnology* **23**, 355708 (2012).
28. Kim, Y. I., Kim, D. & Lee, C. S. Synthesis and characterization of CoFe2O4 magnetic nanoparticles prepared by temperature-controlled coprecipitation method. *Phys. B Condens. Matter* **337**, 42–51 (2003).
29. Cernea, M., Galizia, P., Ciuchi, I. -V., Aldica, G., Mihalache, V., Diamandescu & L. Galassi, C. $CoFe_2O_4$ magnetic ceramic derived from gel and densified by spark plasma sintering. *J. Alloys Compd.* **656**, 854–862 (2016).
30. Imine, S., Shoenstein, F., Mercone, S., Zaghrioui, M., Bettahar, N. & Jouini, N. Bottom-up and new compaction processes: A way to tunable properties of nanostructured cobalt ferrite ceramics. *J. Eur. Ceram. Soc.* **31**, 2943–2955 (2011).
31. Aubert, A., Loyau, V., Mazaleyrat, F. & LoBue, M. Uniaxial anisotropy and enhanced magnetostriction of $CoFe_2O_4$ induced by reaction under uniaxial pressure with SPS. *J. Eur. Ceram. Soc.* **37**, 3101–3105 (2017).
32. Millot, N., Le Gallet, S., Aymes, D., Bernard, F. & Grin, Y. Spark plasma sintering of cobalt ferrite nanopowders prepared by coprecipitation and hydrothermal synthesis. *J. Eur. Ceram. Soc.* **27**, 921–926 (2007).
33. Wu, L. N., Jiang, L. Z. & Hong, F. Y. Dielectric and Magnetic Properties of Sintered Cobalt Ferrite Derived from Nanocrystalline Powders. *Adv. Mater. Res.* **476–478**, 726–729 (2012).
34. Munir, Z. A., Anselmi-Tamburini, U. & Ohyanagi, M. The effect of electric field and pressure on the synthesis and consolidation of materials: A review of the spark plasma sintering method. *J. Mater. Sci.* **41**, 763–777 (2006).
35. Suarez, M., Fèrnandez, A., Menèndez, J. L., Torrecillas, R., Kessel, H. U., Hennicke, J., Kirchner, R., Kessel, T. Challenges and Opportunities for Spark Plasma Sintering: A Key Technology for a New Generation of Materials. Sintering Applications, *InTech*, (2013). doi:10.5772/53706.
36. Maglia, F., Tredici, I. G. & Anselmi-Tamburini, U. Densification and properties of bulk nanocrystalline functional ceramics with grain size below 50 nm. *J. Eur. Ceram. Soc.* **33**, 1045–1066 (2013).

37. Anselmi-Tamburini, U., Garay, J. E. & Munir, Z. A. Fast low-temperature consolidation of bulk nanometric ceramic materials. *Scr. Mater.* **54**, 823–828 (2006).
38. Song, Q. & Zhang, Z. J. Shape Control and Associated Magnetic Properties of Spinel Cobalt Ferrite Nanocrystals. *J. Am. Chem. Soc.* **126**, 6164–6168 (2004).
39. Lu, L. T.,Dung, N. T., Tung ì, L. D., Thanh C. T., Qui, O. K., Chuck, N. V., Maenosono, S. & Thanh, N. T. K. Synthesis of magnetic cobalt ferrite nanoparticles with controlled morphology, monodispersity and composition: the influence of solvent, surfactant, reductant and synthetic conditions. *Nanoscale* **7**, 19596–19610 (2015).
40. Pechini, M. P. Method of preparing lead and alkaline earth titanates and niobates and coating method using the same to form a capacitor. (1967).
41. Khanam, S., Zakaria, A. K. M., Ahsan, M. H., Datta, T.K., Aktar, S., Liba, S. I., Hossain, S., Das, A. K., Kamal I., Yunus, S. M., Saha, D. K. & Erikkson, S.-G. Study of the Crystallographic and Magnetic Structure in the Nickel Substituted Cobalt Ferrites by Neutron Diffraction. *Mater. Sci. Appl.* **6**, 332–342 (2015).
42. Pugh, B. K., Kramer, D. P. & Chen, C. H. Demagnetizing Factors for Various Geometries Precisely Determined Using 3-D Electromagnetic Field Simulation. *IEEE Trans. Magn.* **47**, 4100–4103 (2011).
43. Pawley, G. S. Unit-cell refinement from powder diffraction scans. *J. Appl. Crystallogr.* **14,** 357–361 (1981).
44. Maaz, K., Mumtaz, A., Hasanain, S. K. & Ceylan, A. Synthesis and magnetic properties of cobalt ferrite (CoFe2O4) nanoparticles prepared by wet chemical route. *J. Magn. Magn. Mater.* **308**, 289–295 (2007).
45. Toksha, B. G., Shirsath, S. E., Patange, S. M. & Jadhav, K. M. Structural investigations and magnetic properties of cobalt ferrite nanoparticles prepared by sol–gel auto combustion method. *Solid State Commun.* **147**, 479–483 (2008).
46. Fariñas, J. C., Moreno, R., Pèrez, A., Garcìa, M. A., Garcìa-Hernàndez, M., Salvador, M. D. & Borrell, A. Microwave-assisted solution synthesis, microwave sintering and magnetic properties of cobalt ferrite. *J. Eur. Ceram. Soc.* **38**, 2360–2368 (2018).
47 Ji, W., Rehman, S. S., Wang, W., Wang, H., Wang, Y.W., Zhang, J., Zhang, F., & Fu, Z. Sintering boron carbide ceramics without grain growth by plastic deformation as the dominant densification mechanism. *Scientific reports* **5**, 15827 (2015)